EarthArXiv preprint published at Environmental Research Letters (2019-03-26)
DOI: https://iopscience.iop.org/article/10.1088/1748-9326/ab13bf/meta

Extreme weather events in early summer 2018 connected by a recurrent hemispheric wave-7 pattern

Kai Kornhuber[1,2,*], Scott Osprey[1,2], Dim Coumou[3,4], Stefan Petri[3], Vladimir Petoukhov[3], Stefan Rahmstorf[3], Lesley Gray[1,2]

[1]Atmospheric, Oceanic and Planetary Physics, University of Oxford, Oxford, United Kingdom
[2]National Centre for Atmospheric Science, United Kingdom
[3]Earth System Analysis, Potsdam Institute for Climate Impact Research, Member of the Leibniz Association, Potsdam, Germany
[4]Institute for Environmental Studies, Vrije Universiteit Amsterdam, Amsterdam, Netherlands

*E-mail: Kai Kornhuber (kai.kornhuber@physics.ox.ac.uk)

EarthArXiv preprint published at Environmental Research Letters (2019-03-26)
DOI: https://iopscience.iop.org/article/10.1088/1748-9326/ab13bf/meta

Abstract

The summer of 2018 witnessed a number of extreme weather events such as heatwaves in North America, Western Europe and the Caspian Sea region, and rainfall extremes in South-East Europe and Japan that occurred near-simultaneously. Here we show that some of these extremes were connected by an amplified hemisphere-wide wavenumber 7 circulation pattern. We show that this pattern constitutes an important teleconnection in Northern Hemisphere summer associated with prolonged and above-normal temperatures in North America, Western Europe and the Caspian Sea region. This pattern was also observed during the European heatwaves of 2003, 2006 and 2015 among others. We show that the occurrence of this wave 7 pattern has increased over recent decades.

Keywords: Extreme Weather, Heat Waves, Rossby Waves, Teleconnections

1 Introduction

Extreme weather events such as heatwaves and floods are harmful to society and can lead to increased mortality, crop losses, and damage to infrastructure and economy (*1–3*). The European heatwave of summer 2003 is considered one of the most severe natural disasters in recent European history, with the number of excess deaths reaching tens of thousands and sizable losses to agricultural production across Europe (*1*). The persistent Moscow heatwave in July – August 2010 led to 55000 casualties and 30% crop-yield losses in Russia, whilst the Indus-River flood in Pakistan destroyed infrastructure and affected millions of people (*4, 5*). More recently, the record breaking heatwave of summer 2015 caused widespread water shortages, agricultural damages and wildfires throughout Europe (*6*).

While frequency and intensity of heat waves and heavy rainfall events are expected to increase in a warming world due to thermodynamic arguments (*7, 8*), the exact location and duration of these events are more uncertain and largely controlled by the atmospheric circulation, especially at mid-latitudes. Large-scale weather systems typically move eastward, but when the Jetstream strongly meanders this transport can come to a halt (*9*). Meanders in the jet are referred to as Rossby- or planetary waves and previous studies have pointed out that slow moving amplified planetary waves favor the occurrence of extreme weather conditions at mid-latitudes (*10–12*). Such quasi-stationary planetary waves can form (fully or nearly) circum-global teleconnections leading to the co-occurrence of unusual weather across the mid-latitudes (*13–18*). Moreover, the extreme heatwaves of 2003, 2010 and 2015 have been linked to high amplitude planetary waves. These heatwaves coincided with weather extremes occurring in other regions of the Northern Hemisphere (*12*).

Early summer 2018 witnessed several record-breaking and persistent heat and rainfall extremes occurring near simultaneously in the Northern Hemisphere (NH) mid-latitudes (*19–21*). These extremes include all-time temperature records measured in North America (e.g. Los Angeles and Montreal), in Western Europe (e.g. Glasgow, Belfast), the Caucasus (Tblisi, Yerevan) and Siberia as well as heavy rainfall in the Balkans and over Japan during two weeks in late June and early July.

EarthArXiv preprint published at Environmental Research Letters (2019-03-26)
DOI: https://iopscience.iop.org/article/10.1088/1748-9326/ab13bf/meta

Here we analyse the role of the atmospheric circulation in setting favorable locations of extreme weather events in early Summer 2018 and show that they were part of a recurrent wave-7 pattern (*18*). This wave-7 pattern is shown to constitute a recurrent teleconnection in Northern Hemisphere summer associated with persistent and above-normal temperatures in North America, Western Europe and the Caspian Sea region. We provide evidence that this pattern was also active during past episodes of extreme weather events, including the extreme summer heatwaves of 2003, 2006 and 2015 among others (*12*, *22*, *23*). Furthermore, we show that the identified pattern has increased in frequency and persistence over recent decades.

2 Data and Methods

Daily wind and temperature data were taken from the archives of the National Oceanic and Atmospheric Administration (NOAA, NCEP-NCAR reanalysis (*24*)). In order to avoid spurious trends due to the introduction of satellite-measurements in the late seventies, we limited the analysis to years 1979 – 2018. Wind fields and surface temperature anomaly fields are of a 2.5°x2.5° lat./lon. resolution and precipitation fields are 0.5°x0.5° resolution.

Phase velocities shown in Fig. 2e were determined using a fourth-order accurate numerical approximation of the transient derivative of phase based on daily data following Coumou et al. 2014 (3). In a second step 15-day running mean values of these daily phase velocities are calculated. Spectral decomposition of meridional wind at 300 mb to determine phase and amplitude of Rossby-waves was done using a fast Fourier transformation applied on the mid-latitude band averaged over 37.5° N – 57.5° N (*9*). The surface temperature composite anomaly field (Fig. 4a) was compiled using weekly temperature anomaly fields based on grid-point-wise detrended daily surface temperature fields. Statistical significance was assessed by comparing high amplitude events (>1.5 σ, where σ refers to standard deviation above mean) with the mean of all remaining weeks using a two sided t-test and an adjusted p-value determined by false discovery rate testing (FDR)(*25*).

3 Results

At the end of June, early July 2018 temperatures were anomalously high in specific regions of the Northern Hemisphere, namely the West-Coast of the US, Eastern Canada, western Europe including Scandinavia, the Central Asian regions around and to the North of the Caspian Sea and Siberia (Fig. 1a and Fig. 2a). Over the same time the mid-latitudinal upper tropospheric circulation was characterized by a strongly meandering jet that encircled the northern hemisphere in a regular pattern (Fig. 1b). The circulation regime of summer 2018 was remarkable, not only in terms of the amplitude and regularity of the wave-pattern but also due to its persistence, lasting for about 2 weeks from late-June to early-July.

EarthArXiv preprint published at Environmental Research Letters (2019-03-26)
DOI: https://iopscience.iop.org/article/10.1088/1748-9326/ab13bf/meta

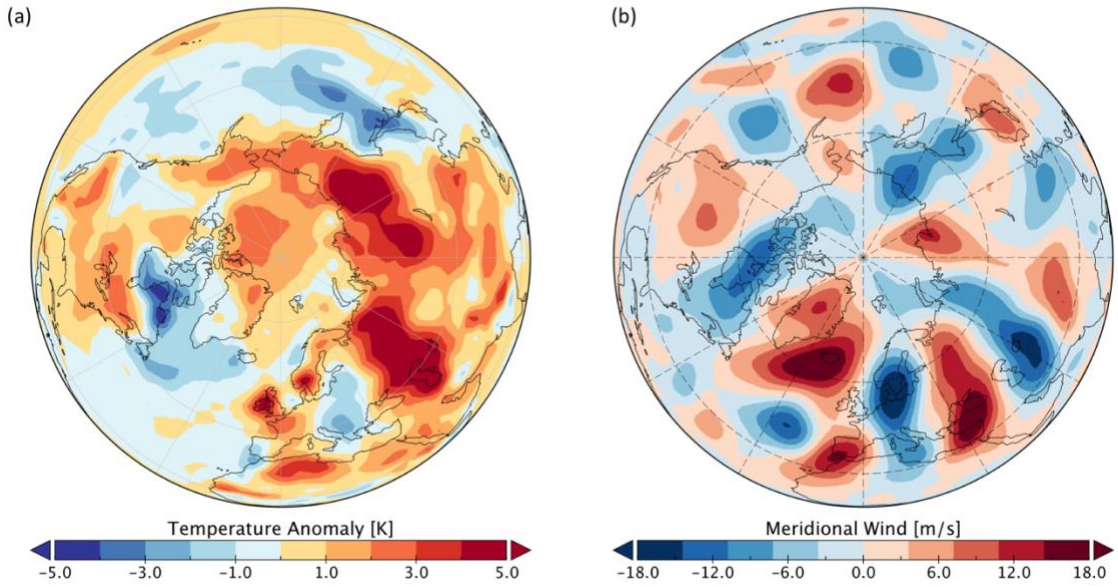

Figure 1. Northern Hemisphere temperature anomalies and stationary Rossby wave pattern in early July 2018. (a) Surface temperature anomalies (from 1981-2010 climatology; 15-day mean, centered on July 1st 2018). Oceans are masked in transparent grey. (**b)** As (a) but for meridional wind V (m s^{-1}) in the upper troposphere (250 mb). Dashed lines indicate the longitudes and latitudes grid at 30° separation.

Figure 2b shows the onset and persistence of the wave pattern as a Hovmöller plot (longitude vs. time) of the meridional winds averaged over the mid-latitudes (37.5°N-57.5°N, with the timing and longitude of persistent extreme weather events superimposed. Here, persistent heat extremes shown in Fig. 2b are defined using the 0.995 percentile threshold determined per grid-point based on detrended daily temperature anomalies (June-July 1979-2018, also see sensitivity analysis Fig.S11). Precipitation fields contain many 'zeros' and thus distributions of daily rain are highly skewed making thresholds based on percentiles challenging. Record statistics are commonly used when analysing precipitation extremes (*8*). Here we define precipitation extremes as the highest value measured at a grid-point in June-July 1979-2018. Only events that were persistent in time (i.e. meeting the extreme weather conditions for $t \geq 2$ days) in the mid-latitude (heat: 37.5°N – 57.5°N, rain: 35.25°N - 57.75°N) land-areas were considered.

In general, the westerly circulation is baroclinic, meaning that there is a displacement between the circulation at upper and lower pressure levels. However, during episodes of amplified planetary waves the atmospheric circulation can be considered as near-barotropic, thus circulation patterns are vertically aligned (*9*) (also see Fig. S12). In such a situation, the longitudinal position of southward and northward meridional winds in Fig. 2b can be understood as alternating troughs (southward followed by northward wind) and ridges (northward followed by southward wind) that relate to local cyclonic and anti-cyclonic circulation, respectively.

EarthArXiv preprint published at Environmental Research Letters (2019-03-26)
DOI: https://iopscience.iop.org/article/10.1088/1748-9326/ab13bf/meta

Consistent with this circulation, heat extremes (red diamonds in 2b) are generally located below a ridge, associated with anticyclonic conditions. In contrast, precipitation extremes (blue triangles) are generally below a trough, i.e. cyclonic conditions. While two thirds of the detected extremes are consistent with this description, there are some exceptions. Events not consistent with this behaviour include heat extremes over the North American west coast (~125°W) during June and over East Asia (~135°E in early June and the precipitation extremes over central North America mid-July (~120°W) and central Asia (~125°E) end of July. Relatively low meridional wind speeds in these regions suggest that these events might not be directly linked to the large-scale circulation (Fig. S6a). The mid-latitude circulation can be quantified in terms of Rossby waves by decomposing it into its principal wave components using a Fourier transformation (*10*, *26*). Starting at the end of June, a quasi-stationary wavenumber 7 (wave-7 from hereon) Rossby wave evolves (Fig. S3a, b) to large amplitude (Fig. 2b,c, Fig. S3c), near-stationary phase position (Fig. 2d) and near-zero phase speed (Fig. 2e). Although early Summer 2018 saw several persistent heat and rainfall extremes, simultaneous extremes in the mid latitudes occurred mostly during the period of amplified wave-7, specifically over the Eurasian continent (Fig. 2b). Those include the heat extremes over the British Isles, the rainfall extreme over SE Europe, the heat extreme over the Caspian Sea region and the heat extremes over Siberia (*19–21*). The precipitation extreme over Japan also occurring within this period was linked to an ex-tropical storm but was likely influenced by the large-scale circulation (see SI for details).

Wave-7 shows some unique behavior: it exhibits a persistent and preferred phase position when its amplitude increases (*18*) (also see Fig. S4), creating a circumglobal teleconnection pattern in NH summer (Fig. 3a,b). This is consistent with the work from Branstator et al. (*27*) and Ding and Wang (*16*) who showed that zonally elongated zonal winds (see Fig. S9) can act as waveguides for planetary waves leading to co-variability in far-away regions (*28*). The amplitude starts to increase from mid-June, exceeding the 1.5 standard deviation threshold by the end of June (Fig. 2c) and persists at that high level until early July. Concurrent with the rising amplitude, the wave shifts into its preferred phase-position (indicated by the dashed red lines in Fig. 2d, also see Fig. S4) where it persists for almost 3 weeks. The absolute phase speed of wave-7 thus slows down reaching almost zero when the wave enters its preferred phase position (Fig. 2e).

EarthArXiv preprint published at Environmental Research Letters (2019-03-26)
DOI: https://iopscience.iop.org/article/10.1088/1748-9326/ab13bf/meta

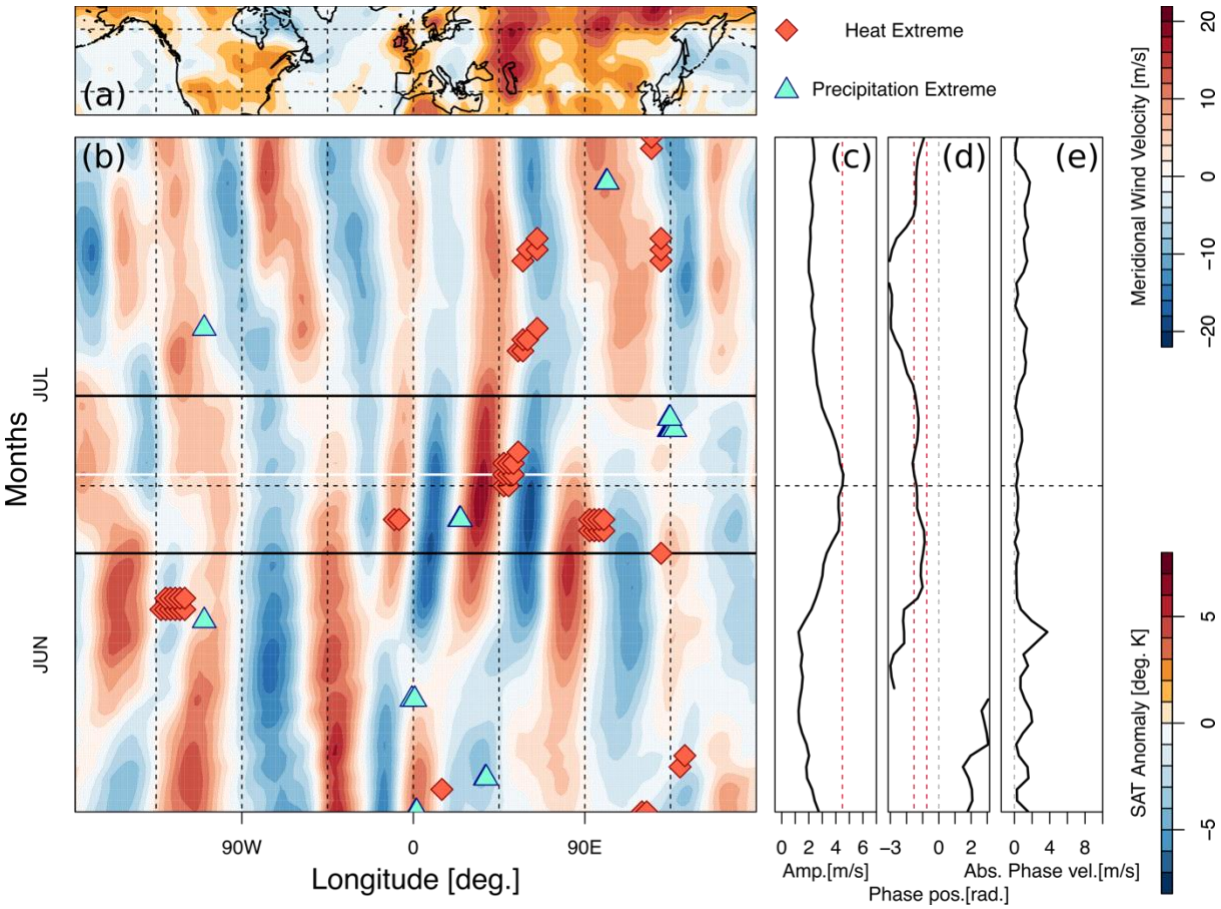

Figure 2. Time evolution of persistent wave-7 circulation pattern. (a) NH surface air temperatures (15-day mean centered on July 1st 2018). **(b)** Hovmöller (longitude-time) time evolution of the mid-latitude (averaged over 37.5°N – 57.5°N) 300 mb meridional winds. A stationary wave-7 pattern evolves during mid-June. The location and timing of persistent extreme events are marked by orange diamonds (heat extreme) and blue triangles (precipitation extreme). July 1st is marked by a horizontal white line, while the 15-day mean period is marked by horizontal black lines. The horizontal dashed lines mark the last day of June, while the vertical dashed lines separate the longitudes at 45° steps. **(c)** The amplitude of wave 7 increases and approaches the 1.5 σ (red dashed line) end of June / early July when heat records are broken across the mid-latitudes. **(d)** Phase of wave-7 (radians). The phase becomes locked within its preferred position (marked by red dashed lines) by end of June. **(e)** Phase speed of wave 7 (m s^{-1}). The phase speed slows down in concert with the increasing amplitude and the phase locking of wave-7.

The occurrence of this specific circulation pattern was not unique to June/July 2018. The hemispheric circulation associated with amplified wave-7 is a recurrent pattern observed in other years. As a consequence of its preferred phase, it exhibits spatially confined troughs and ridges which then persist over specific regions (Fig. 3) (*18*, *29*). A characteristic circumglobal pattern of alternating temperature anomalies thus arises across the mid-latitudinal belt with significantly elevated surface temperatures over central North America, Western/Central Europe and the Caspian Sea region (Fig. 3a). Here, high amplitude wave-7 events are defined by weeks in JJA where the amplitude exceeds the +1.5σ threshold (the pattern however is independent of the exact choice of threshold; see Fig. S5). In the regions identified above,

EarthArXiv preprint published at Environmental Research Letters (2019-03-26)
DOI: https://iopscience.iop.org/article/10.1088/1748-9326/ab13bf/meta

anomalous circulation arising from the wave-7 circumglobal teleconnection can then intensify the normal summer temperatures, contributing to heat waves on weekly to monthly time scales.

To quantify the similarity of the wave-7 pattern (Fig. 3b) with the mid-latitude meridional wind in 2018, we compute their hemispheric spatial correlation in the midlatitudes (57.5-37.5°N) also including separate sectors (Eastern hemisphere: 30W-150E, Western hemisphere: 150°E-30°W) (Fig. S2). During the phase-locked period (end of June, early July), the spatial correlations ρ peak above a level of 0.4, (statistically significant at the 99% confidence level) and remain over a threshold above 1.5 σ (Fig.S2c). Analysis of the separate sectors reveals that this is mainly due to the very high agreement over the eastern hemisphere (30W-150E, $\rho > 0.8$), although the western hemisphere nearly exceeds the 1.5σ threshold as well. In agreement with summer 2018, notable past amplitude wave-7 events coincide with heat extremes in central Western Europe and the Caspian Sea region as suggested by the surface temperature anomaly map (Fig. 3a), among them the heatwaves of 2003, 2006, 2012 and 2015 (*12*, *18*) (also see Fig. S6, Table S1).

Over recent decades the number of *phase-locked* wave-7 events (here defined as weeks with above average wave-7 amplitude within its preferred position, see Fig. S4) have increased significantly (95% confidence interval, Fig. 4b). Prior to 1999 there were no summers with two or more consecutive weeks of a wave 7 phase-locked circulation, but since then these have occurred (Table S2). Thus, the persistence of such situations appears to have increased. In fact, the average duration has doubled from about one to two weeks per year, while the number of years with more than two events per summer shows an almost eight-fold increase (Fig. S7). Although the trends are always upward, i.e. independent of the amplitude threshold used, their significance is sensitive to the amplitude threshold due to the reduction in ensemble size for high amplitudes (Fig. 4b). The number of wave-7 events (i.e. weeks with a high-amplitude wave-7 *irrespective* of its phase position) do not show statistically significant upward trends for different thresholds used (Fig. 4a). A statistically significant upward trend in the observed amplitude of summertime wave-7 is only detected when data from the pre-satellite period is included (Fig. S7). The more pronounced trends in *phase-locked* events (Fig. 4b), compared to high-amplitude events (Fig. 4a) suggests that it is the phase-locking itself that has increased. In general, these trends can simply reflect multi-decadal variability in the earth system given that the satellite record is relatively short. Nevertheless, an enhanced land-ocean temperature contrast as a consequence of amplified land warming provides a physical mechanism for such waves to become preferentially phase-locked. Such temperature contrast create an increased zonal temperature gradient at the coastlines and provide a stationary vorticity source that triggers and maintains atmospheric waves (*30*, *31*). It is therefore possible that the relative position of land and ocean areas in the mid-latitudes with high values of dT/dx over the continental West-coasts could favour a hemispheric wave 7 pattern (*32*). Such contrast would further enhanced by the cooling trend of northern Atlantic sea surface temperatures linked to a slowdown of the Atlantic Meridional Overturning Circulation (*33*) and implicated in past European heat extremes (*23*) but this needs further investigation.

EarthArXiv preprint published at Environmental Research Letters (2019-03-26)
DOI: https://iopscience.iop.org/article/10.1088/1748-9326/ab13bf/meta

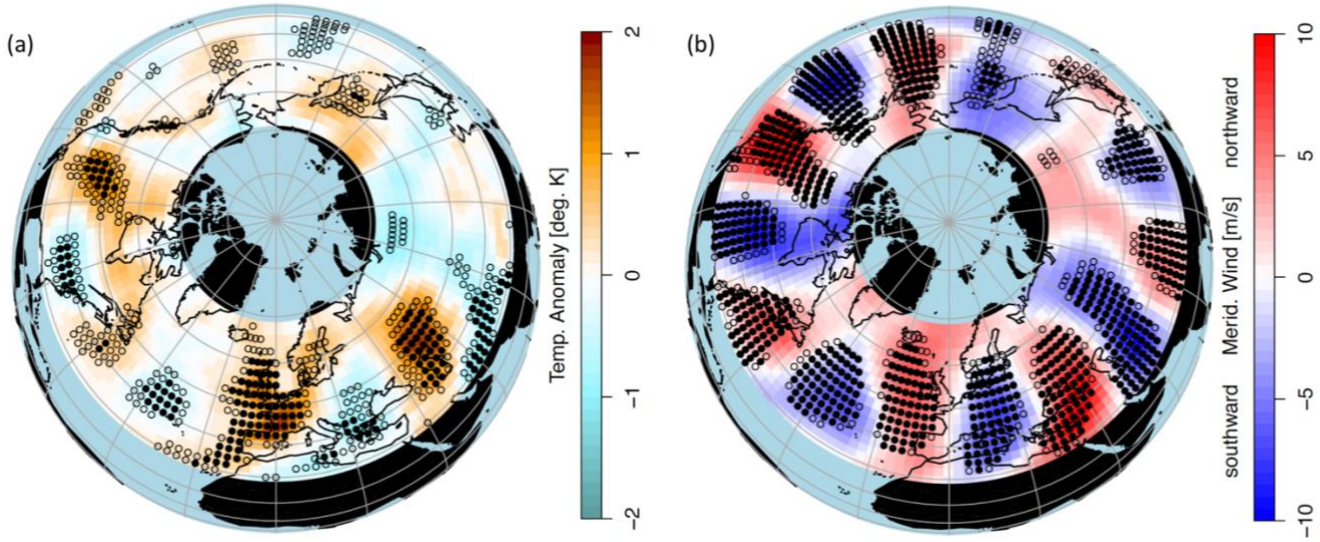

Figure 3. Composite plots of wave-7 events: A recurrent teleconnection. (a) Composite plot of surface temperature anomalies over the NH mid-latitudes (30°N - 67.5°N) during weeks of high wave-7 amplitudes (>1.5σ, N: 43 weeks, see Tab. S1) in summer (JJA) over the NH mid-latitudes (30°N - 67.5°N) observed over the period 1979 - 2017. **(b)** 300 mb meridional wind speeds (northward: red; southward: blue) during those events. The filled stippling in (**a**) and (**b**) indicates grid-cells with significant deviations from JJA climatology using a significance test that accounts for the false discovery rate (FDR) associated with multiple testing (*25*), while the grid-points marked with hollow stippling indicate local significance.

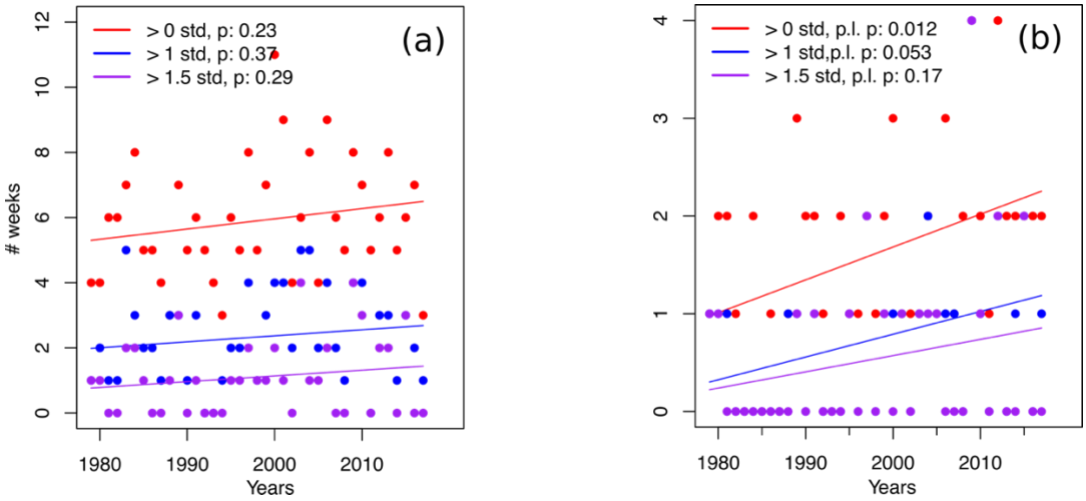

Figure 4. Recent trends in the occurrence of the wave-7 teleconnection. **(a)** Number of weeks per summer season (JJA, 1979-2017) with wave-7 amplitude above average (>0σ)**,** 1σ and 1.5σ irrespective of phase position. (**b)** Number of weeks per summer season (JJA) where wave-7 is in its preferred phase position (see Fig. S4) and the amplitude of wave-7 is above average (>0σ), >1 σ and >1.5σ.

EarthArXiv preprint published at Environmental Research Letters (2019-03-26)
DOI: https://iopscience.iop.org/article/10.1088/1748-9326/ab13bf/meta

4 Discussion

Extreme weather events such as the heatwaves observed in summer 2018 can be the product of several compounding factors acting together. For example it has been shown that the extreme heatwaves in Europe (2003) and Russia (2010) were preceded by very low soil moisture content due to an anomalously dry spring season (*22*, *34*, *35*). Similarly, during April-May 2018, soil moisture feedbacks may also have contributed to the magnitude and persistence of the observed heatwaves (*34*). Generally, heat waves are becoming more intense as the mean climate warms due to increasing greenhouse gas (GHG) concentrations (*36*). GHG warming also leads to enhanced water-holding capacity of the air (Clausius-Clapeyron), fueling heavier rainfall events(*8*). For these thermodynamic reasons, it is thus likely that the observed extremes in 2018 have in part been fueled by the global warming trend. However the timing, duration and location of a specific extreme weather event, can be largely controlled by the large scale circulation, especially at mid-latitudes (*37*).

While the direct response of weather extremes to thermodynamic drivers is generally well understood, large uncertainty remains of the indirect response from the changing atmospheric circulation under a warmer climate (*37–41*). Dynamical changes in the circulation have been proposed to explain the increase in persistence and magnitude of recent summer extremes that are otherwise unaccounted for using simple thermodynamic arguments (*41*, *42*). This arguments are particularly relevant in the case of Western and Central Europe as well as the Southern Central US being repeatedly struck by devastating heatwaves (*22*, *43–46*). Summer storm tracks have been weakening over recent decades (*47*) which likely influences planetary wave behaviour. In boreal summer the amplitude of synoptic Rossby waves (waves 5 and higher) have indeed been increasing recently, in agreement with our results (*48*). However, others studies have shown that upward trends over a relatively short period are difficult to assess (*49*) and traditional blocking indices also show no changes in summer (*50*).

The regions for which an increase in the persistence of regional weather regimes was identified (Europe and Western Asia) match those related to the wave-7 teleconnection pattern (*51*). Planetary wave resonance has been discussed as a potential mechanism to generate high amplitude synoptic wave patterns in boreal summer (*9*, *12*, *18*) and necessary conditions were present in June-July 2018 as well (also see discussion in SI). Recent trends in the zonal temperature profile due to anthropogenic climate change might favour resonance conditions (*32*). This temperature profile is characterized by enhanced land warming over high latitudes favouring the formation of an Arctic front jet, and subsequent double jet in the zonal mean (*12*, *32*). In fact, for 2018 such Arctic front jet is clearly visible over the Eurasian continent (Fig. S9), which might be the reason that planetary wave patterns were specifically amplified and persistent.

5 Conclusion

In summary, we have shown that the summer 2018 featured a series of nearly simultaneous extreme weather events that coincided in time and space with a circumglobal teleconnection constituted by an amplified Rossby wave (wave-7) in the mid-latitude jet stream specifically

over Eurasia. These extremes include the heat-records of June/July broken in Western Europe and Caspian Sea region, as well as the extreme and devastating rainfall events in South-East Europe. Tropical ENSO variability in 2018 was in a neutral state and thus unlikely to be an important factor behind the extreme weather events in the NH. This recurrent wave-7 circulation pattern conducive for heat waves acts in addition to the thermodynamically driven increase in heat, creating possibilities for very-extreme heat waves, specifically in the identified regions: Western Europe, North America and Caspian Sea region. We show that this circumglobal teleconnection pattern has increased in frequency and persistence in recent years. Given the high impacts of these extremes in terms of mortality, morbidity and agricultural losses, this presents major risks for society and global food production in particular, since the main breadbasket regions are located in the mid-latitudes. Further research is required to fully understand the combination of factors that trigger these observed wave events, and what determines their preferred phase position, so that predictability of future extreme events can be improved.

Acknowledgements

The federal state of Brandenburg is acknowledged for supporting the used high-performance computing resources. **Funding**: This work was supported by the UK Natural Environment Research Council (NERC) National Centre for Atmospheric Science (NCAS) and NERC grants NE/P006779/1 and NE/N018001/1 (K.K., L.G. and S.O.) and by the German Federal Ministry of Education and Research (BMBF) and by the Netherlands Organisation for Scientific Research (NWO) (D.C). **Author contributions**: K.K., S.O., D.C., L.G. conceptualised the paper. K.K. undertook the analysis. All authors contributed to the writing of the paper. **Competing Interests**: The authors declare no competing interests. **Data and materials availability**: The data used in this study can be obtained from NCEP-NCAR websites or via the UK Centre for Environmental Data Analysis (CEDA)

References:

1. D. Mitchell *et al.*, Attributing human mortality during extreme heat waves to anthropogenic climate change. *Environ. Res. Lett.* **11**, 74006 (2016).

2. C. Lesk, P. Rowhani, N. Ramankutty, Influence of extreme weather disasters on global crop production. *Nature*. **529**, 84–87 (2016).

3. L. Wenz, A. Levermann, Enhanced economic connectivity to foster heat-stress-related losses. *Sci. Adv.* **2**, e1501026 (2016).

4. D. Coumou, S. Rahmstorf, A decade of weather extremes. *Nat. Clim. Chang.* **2**, 1–6 (2012).

5. S. Russo *et al.*, Magnitude of extreme heat waves in present climate and their projection in a warming world. *J. Geophys. Res. Atmos.* **119**, 500–12 (2014).

6. NOAA, State of the Climate: Global Climate Report for 2015 (2016), (available at https://www.ncdc.noaa.gov/sotc/global/201513).

7. D. Coumou, A. Robinson, Historic and future increase in the global land area affected by monthly heat extremes. *Environ. Res. Lett.* **8**, 034018 (2013).

8. J. Lehmann, D. Coumou, K. Frieler, Increased record-breaking precipitation events under global warming. *Clim. Change*. **132**, 501–515 (2015).

9. V. Petoukhov, S. Rahmstorf, S. Petri, H. J. Schellnhuber, Quasiresonant amplification of planetary waves and recent Northern Hemisphere weather extremes. *Proc. Natl. Acad. Sci.* **110**, 5336–41 (2013).

10. J. A. Screen, I. Simmonds, Amplified mid-latitude planetary waves favour particular regional weather extremes. *Nat. Clim. Chang.* **4**, 704–709 (2014).

11. D. Coumou, V. Petoukhov, S. Rahmstorf, S. Petri, H. J. Schellnhuber, Quasi-resonant circulation regimes and hemispheric synchronization of extreme weather in boreal summer. *Proc. Natl. Acad. Sci.* **111**, 12331–12336 (2014).

12. K. Kornhuber, V. Petoukhov, S. Petri, S. Rahmstorf, D. Coumou, Evidence for wave resonance as a key mechanism for generating high-amplitude quasi-stationary waves in boreal summer. *Clim. Dyn.* **49**, 1961–1979 (2017).

13. K. Deng, S. Yang, M. Ting, A. Lin, Z. Wang, An Intensified Mode of Variability Modulating the Summer Heat Waves in Eastern Europe and Northern China, 361–369 (2018).

14. W. K. M. Lau, K.-M. Kim, The 2010 Pakistan Flood and Russian Heat Wave: Teleconnection of Hydrometeorological Extremes. *J. Hydrometeorol.* **13**, 392–403 (2012).

15. S. Saeed, N. Van Lipzig, W. A. Müller, F. Saeed, D. Zanchettin, Influence of the circumglobal wave-train on European summer precipitation. *Clim. Dyn.* **43**, 503–515 (2014).

16. Q. Ding, B. Wang, Circumglobal teleconnection in the Northern Hemisphere summer. *J. Clim.* **18**, 3483–3505 (2005).

17. H. Teng, G. Branstator, H. Wang, G. A. Meehl, W. M. Washington, Probability of US heat waves affected by a subseasonal planetary wave pattern. *Nat. Geosci.* **6**, 1056–1061 (2013).

18. K. Kornhuber *et al.*, Summertime Planetary Wave-Resonance in the Northern and Southern Hemisphere. *J. Clim.* **30**, 6133–6150 (2017).

19. NOAA, "State of the Climate: Global Climate Report for July 2018" (2018), (available at https://www.ncdc.noaa.gov/sotc/global/201807).

20. NOAA, "State of the Climate: Global Climate Report for June 2018" (2018), (available at https://www.ncdc.noaa.gov/sotc/global/201806).

21. International Federation of Red Cross and Red Crescent Societies, "Information Bulletin no. 1 Flash floods in Europe" (2018).

22. E. Black, M. Blackburn, G. Harrison, B. Hoskins, J. Methven, Factors contributing to the summer 2003 European heatwave. *Weather*. **59**, 217–223 (2004).

23. A. Duchez *et al.*, Drivers of exceptionally cold North Atlantic Ocean temperatures and their link to the 2015 European heat wave. *Environ. Res. Lett.* **11**, 074004 (2016).

24. Kalnay et al., The NCEP/NCAR 40-year reanalysis project. *Bull. Am. Meteorol. Soc.*, 437–470 (1996).

25. D. Wilks, " The Stippling Shows Statistically Significant Grid Points ." *Bull. Am. Meteorol. Soc.* **97**, 2263–2274 (2016).

26. D. Coumou, K. Kornhuber, J. Lehmann, V. Petoukhov, in *Climate Extremes: Patterns and*

Mechanisms, S.-Y. S. Wang, J.-H. Yoon, C. C. Funk, R. R. Gillies, Eds. (John Wiley & Sons, First Edit., 2017), pp. 61–73.

27. G. Branstator, Circumglobal Teleconnections, the Jet Stream Waveguide, and the North Atlantic Oscillation. *J. Clim.* **15**, 1893–1910 (2002).

28. G. Branstator, H. Teng, Tropospheric Waveguide Teleconnections and Their Seasonality. *J. Atmos. Sci.* **74**, 1513–1532 (2017).

29. J. Zhang, J. Yuanchun, C. Haishan, W. Zhiwei, Double-mode adjustment of Tibetan Plateau heating to the summer circumglobal teleconnection in the Northern Hemisphere. *Int. J. Climatol.* (2017), doi:10.1002/joc.5201.

30. T. A. Shaw, A. Voigt, Tug of war on summertime circulation between radiative forcing and sea surface warming. *Nat. Geosci.* **8**, 560–566 (2015).

31. B. J. Hoskins, D. J. Karoly, The Steady Linear Response of a Spherical Atmosphere to Thermal and Orographic Forcing. *J. Atmos. Sci.* **38**, 1179–1196 (1981).

32. M. E. Mann *et al.*, Influence of Anthropogenic Climate Change on Planetary Wave Resonance and Extreme Weather Events. *Sci. Rep.* **7**, 45242 (2017).

33. L. Caesar, S. Rahmstorf, A. Robinson, G. Feulner, Observed fingerprint of a weakening Atlantic Ocean overturning circulation. *Nature*. **556**, 191–196 (2018).

34. E. M. Fischer, S. I. Seneviratne, D. Lüthi, C. Schär, Contribution of land-atmosphere coupling to recent European summer heat waves. *Geophys. Res. Lett.* **34**, L06707 (2007).

35. D. G. Miralles, A. J. Teuling, C. C. van Heerwaarden, J. Vilà-Guerau de Arellano, Mega-heatwave temperatures due to combined soil desiccation and atmospheric heat accumulation. *Nat. Geosci.* **7**, 345–349 (2014).

36. D. Coumou, A. Robinson, Historic and future increase in the global land area affected by monthly heat extremes. *Environ. Res. Lett.* **8**, 034018 (2013).

37. T. G. Shepherd, Atmospheric circulation as a source of uncertainty in climate change projections. *Nat. Geosci.* **7**, 703–708 (2014).

38. J. Cohen *et al.*, Recent Arctic amplification and extreme mid-latitude weather. *Nat. Geosci.* **7**, 627–637 (2014).

39. E. A. Barnes, J. A. Screen, The impact of Arctic warming on the midlatitude jet-stream: Can it? Has it? Will it? *Wiley Interdiscip. Rev. Clim. Chang.* (2015) (available at http://doi.wiley.com/10.1002/wcc.337).

40. B. Hoskins, T. Woollings, Persistent Extratropical Regimes and Climate Extremes. *Curr. Clim. Chang. Reports*. **1**, 115–124 (2015).

41. R. M. Horton, J. S. Mankin, C. Lesk, E. Coffel, C. Raymond, A Review of Recent Advances in Research on Extreme Heat Events. *Curr. Clim. Chang. Reports*. **2**, 242–259 (2016).

42. J. Luterbacher *et al.*, European Seasonal and Annual Temperature Variability, Trends, and Extremes Since 1500. *Science (80-.).* **303**, 1499–1503 (2004).

43. A. Hoy, S. Hänsel, P. Skalak, Z. Ustrnul, O. Bochníček, The extreme European summer of 2015 in a long-term perspective. *Int. J. Climatol.*, 1–20 (2016).

44. M. Rebetez, O. Dupont, M. Giroud, An analysis of the July 2006 heatwave extent in Europe

compared to the record year of 2003. *Theor. Appl. Climatol.* **95**, 1–7 (2009).

45. M. Hoerling, J. K. Eischeid, X. Quan, T. Xu, Explaining the record US warmth of 2006. *Geophys. Res. Lett.* **34**, 1–4 (2007).

46. N. S. Diffenbaugh, M. Scherer, Likelihood of July 2012 U.S. temperatures in preindustrial and current forcing regimes. *Bull. Am. Meteorol. Soc.*, 6–9 (2013).

47. D. Coumou, J. Lehmann, J. Beckmann, The weakening summer circulation in the Northern Hemisphere mid-latitudes. *Science (80-.).* **348**, 324–327 (2015).

48. S.-Y. Wang, R. E. Davies, R. R. Gillies, Identification of extreme precipitation threat across midlatitude regions based on short-wave circulations. *J. Geophys. Res. Atmos.* **118**, 11059–11074 (2013).

49. J. A. Screen, I. Simmonds, Exploring links between Arctic amplification and mid-latitude weather. **40**, 959–964 (2013).

50. T. Woollings *et al.*, Blocking and its Response to Climate Change. *Curr. Clim. Chang. Reports*, 1–14 (2018).

51. D. E. Horton *et al.*, Contribution of changes in atmospheric circulation patterns to extreme temperature trends. *Nature*. **522**, 465–469 (2015).